# Next generation DNA sequencing of atypical choroid plexus papilloma of brain: Identification of novel mutations in a female patient by Ion Proton

MOHIUDDIN M. TAHER[1,2], AMAL ALI HASSAN[3,4], MUHAMMAD SAEED[5], RAID A. JASTANIA[6],
TAHANI H. NAGEETI[7], HISHAM ALKHALIDI[8], GHIDA DAIRI[9], ZAINULARIFEEN ABDULJALEEL[1,2],
MOHAMMAD ATHAR[1,2], ABDELLATIF BOUAZZAOUI[1,2], WAFA M. EL-BJEIRAMI[10] and FAISAL A. AL-ALLAF[1,2]

[1]Department of Medical Genetics, Faculty of Medicine; [2]Science and Technology Unit, Umm-Al-Qura University,
Makkah 21955; [3]Histopathology Division, Al-Noor Specialty Hospital, Makkah 24242, Saudi Arabia; [4]Faculty of Medicine,
Department of Pathology, Al Azhar University, Cairo 11651, Egypt; Departments of [5]Radiology and [6]Pathology, Faculty
of Medicine, Umm-Al-Qura University, Makkah 21955; [7]Department of Radiation Oncology, King Abdullah Medical City,
Makkah 24246; [8]Department of Pathology, College of Medicine, King Saud University, Riyadh 11461; [9]Medicine and
Medical Sciences Research Center, Deanship of Scientific Research, Umm-Al-Qura University, Makkah 21955;
[10]Laboratory Medicine and Molecular Diagnostics Unit, King Abdullah Medical City, Makkah 24246, Saudi Arabia

**Abstract.** Choroid plexus papilloma (CPP) is a rare benign tumor of the central nervous system that is usually confined to the cerebral ventricles. According to the World Health Organization, CPP corresponds to a grade I atypical CPP (a-CPP); however, it can become more aggressive and reach grade II, which can rarely undergo malignant transformation into a choroid plexus carcinoma (grade III). To the best of our knowledge, identification of these tumors mutations by next generation DNA sequencing (NGS) has not been yet reported. In the present study, NGS analysis of an a-CPP case was performed. Data were analyzed using Advaita Bioinformatics i-VariantGuide and Ion Reporter 5.6 programs. The results from NGS identified 12 novel missense mutations in the following genes: NOTCH1, ATM, STK36, MAGI1, DST, RECQL4, NUMA1, THBS1, MYH11, MALT1, SMARCA4 and CDH20. The PolyPhen score of six variants viz., DST, RECQL4, NUMA1, THBS1, MYHI1 and SMARCA4 were high, which suggested these variants represents pathogenic variants. Two novel insertions that caused frameshift were also found. Furthermore, two novel nonsense mutations and 14 novel intronic variants were identified in this tumor. The novel missense mutation detected in ATM gene was situated in c.5808A>T; p. (Leu1936Phe) in exon 39, and a known ATM mutation was in c.5948A>G; p. (Asn1983Ser). These novel mutations had not been reported in previous database. Subsequently, the quality statistics of these variants, including allele coverage, allele ratio, P-value, Phred quality score, sequencing coverage, PolyPhen score and alleles frequency was performed. For all variants, P-value was highly significant and the Phred quality score was high. In addition, the results from sequencing coverage demonstrated that 97.02% reads were on target and that 97.88% amplicons had at least 500 reads. These findings may serve at determining new strategies to distinguish the types of choroid plexus tumor, and at developing novel targeted therapies. Development of NGS technologies in the Kingdom of Saudi Arabia may be used in molecular pathology laboratories.

*Correspondence to:* Dr Mohiuddin M. Taher, Department of Medical Genetics, Faculty of Medicine, Umm Al-Qura University, Al-Abedia Campus, Makkah 21955, Saudi Arabia
E-mail: taher23223@yahoo.com

*Abbreviations:* a-CPP, atypical choroid plexus papilloma; AT, ataxia-telangiectasia; CNS, central nervous system; CNV, copy number variation; CSF, cerebrospinal fluid; HPF, high-power fields; NGS, next generation DNA sequencing; PICU, pediatric intensive care unit; PolyPhen, polymorphism phenotyping; SNP, single nucleotide polymorphisms; vcf, variant call format

## Introduction

Choroid plexus tumors (CPT) have arisen as papillary neoplasms of choroid plexus in the brain, particularly in children lateral ventricle or in adult fourth ventricle (1). These tumors originate from the epithelium of choroid plexus. They can be benign or malignant and known as choroid plexus papilloma (CPP) or choroid plexus carcinoma (CPC), respectively (2). In children, CPP account for 2-3% of all intracranial tumors, with a median age at diagnosis around 3.5 years old (3) and an annual incidence of 0.3 cases

per million. This neoplasm outnumbers CPC by a factor of 5:1 (4). The tumor is commonly located in the lateral ventricle, and the main symptom is an elevated intracranial pressure. Histopathological characteristics observed in CPP are essentially calcification, hemorrhage, hyalinization, oncocytic changes, and other presenting symptoms, including headache, diplopia and ataxia from hydrocephalus (5). Direct mechanical obstruction of cerebrospinal fluid (CSF) flow, hemorrhage that causes arachnoid granulation obstruction, and CSF overproduction can stimulate the development of hydrocephalus, and occasionally lead to CSF leaks out from the nose (6). Metastasis of CPP tumors exists; however, extensive metastasis has only been reported when tumors are malignant (7). Histologically, CPP corresponds to grade I, according to the World Health Organization (WHO); however atypical CPP (a-CPP) become more aggressive and reach grade II. It very rarely transforms into grade III-CPC (4). Although CPPs are commonly benign, histological analysis is not always predictive of their behavior. Molecular and genetics analyses may therefore be helpful for diagnosis and tumor prognosis (7,8).

Increased prevalence of CPC due to R337H mutation of the germline gene tumor protein p53 (TP53) in southern Brazil was reported (9). Custodio *et al* (9) demonstrated for the first time that this mutation is responsible for 63% of CPC cases in children, which indicates a higher incidence of CPC in southern Brazil. This study including 22 children with CPC and 7 children with CPP was based on PCR-RFLP and confirmed by sequencing exon 10 of TP53. They reported that all CPP cases (7/7) were negative for R337H (9). A recent study using whole exome sequencing demonstrated that homologous recombination deficiency, amplification of mesenchymal-epithelial transition (MET) and loss of retinoblastoma susceptibility gene were observed in two cases of CPC (malignant peripheral nerve sheath tumor sheath tumor) (10). Conversely with other types of brain tumor, extensive mutation profiling in CPT cases were not previously attempted by next generation DNA sequencing (NGS) methods. However, gene expression profiles using DNA micro-arrays, Sanger sequencing of TP53 gene, copy number variation and DNA methylation studies in CPT were attempted (11,12). It has been reported that mutations in hSNF5/INI1 are associated with CPCs, and one mutation in the SNF5/INI1 gene in one case of a-CPP is known (13). However, Mueller *et al* (14) have reported that there is no evidence of hSNF5/INI1 point mutations by SSCP analysis in CPP. Furthermore, hSNF5/INI1 (SMARCB1) gene serves an integral role in chromatin remodeling (15). SMARCB1 is an invariant of the SWI/SNF chromatin-remodeling complex and serves an important role in transcriptional regulation (16). Patients with rhabdoid tumors, CPC, epithelioid sarcoma and peripheral primitive neuroectodermal tumor exhibit a loss of SMARCB1 expression either by exons duplications or deletions, although the number of cases with SMARCB1 mutations are limited (17).

Mutations in ATM gene are associated with breast cancer and several forms of leukemia and lymphomas (18). However, no association between the development of brain tumors and ATM gene mutations has been yet established. A previous study demonstrated an association between astrocytoma development and familial ataxia-telangiectasia (AT) in an 8-year-old patient (19). A previous study using Sanger sequencing reported a compound heterozygote for two novel mutations: c.3291delC (p.Phe1097fs) at exon 25 and c.8198A>C (p.Gln2733Pro) at exon 58 in the ATM gene of patient with AT and with a cerebellar astrocytoma (20). Another study using next-generation targeted exome sequencing revealed a frameshift mutation p. L2493fs c.4477_4478CTCT in a patient with astroblastoma, and a missense mutation p. (Val410Ala) in the ATM gene in a patient with astrocytoma from the same group (21). To the best of our knowledge, molecular genetics investigations, particularly ATM gene mutations in patients with CPP and CPC by DNA sequencing using NGS methods have not yet been investigated, and the mutation profiling of these tumors remains unclear. The present study was the first to report NGS analysis of an a-CPP tumor on Ion Proton using cancer comprehensive panel genes and identification of a novel and known mutations.

**Materials and methods**

The present study was approved by the Institutional Review Board (IRB) for Bioethics Committee of the King Abdullah Medical City (IRB no. 14-140) and performed in accordance with the principles of the Declaration of Helsinki. Informed consent was obtained from the guardian of the patient prior to the study. The diagnosis was made following radiological, histopathological and immunological examinations. Tumors were classified based upon similarity to the constituent cells of the central nervous system (CNS), including astrocytes, oligodendrocytes, ependymal and glial cells, mitotic activity was assessed by counting mitoses in 10 randomly selected high-powered fields at x40 magnification using Nikon Eclipse Ci series Upright Light-microscope (Nikon Corporation). and the proliferation index was assessed by Ki-67 staining as per the WHO grading system (4). Clinicopathological and demographic characteristics of the patient were obtained and further analyzed for the present study.

*Radiology and histopathological analysis.* A CT scan of the brain was performed using a multi-slice CT (MSCT), using a 64-detector-row scanner. The use of CT allowed visualization of detailed images of the soft tissues in the body in 3D as well as in multiplanar reconstructions. Images were captured using 5 mm-thick sections on a GE Medical Systems, light speed VCT, 64-slice multidetector CT (MDCT). High quality images were processed at low dose performance on Volara™ digital Data Acquisition System.

The excised tumor was fixed at room temperature in 4% buffered formalin for 12-24 h maximum, then routinely processed and paraffin embedded. The 4-$\mu$m-thick sections were prepared on clear ground glass microscope slides with ground edges, and routinely stained using Dako Reagent Management System (DakoRMS) with hematoxylin for 3 min and eosin for 30 sec at 25°C each on a Dako Coverstainer (Agilent Technologies). For immunohistochemistry studies, sections were collected on Citoglas adhesion microscope slides (Citotest). Briefly, the tissue sections were deparaffinized with EZ Prep (cat. no. 950-102; Ventana Medical Systems, Inc.) at 60°C for 1 h. After the antigen retrieval of the deparaffinized sections using tris-(hydroxymethyl)-aminomethane-based antigen retrieval reagent (Ventana Medical Systems, Inc.) at

95-100˚C was performed for 30 min by mild cell condition-I protocol using cell conditioning solution (CC1) Ventana Catalog Number 950-124 and the immunohistochemistry was performed using the Ventana BenchMark XT automated stainer (Ventana Medical Systems, Inc.). CONFIRM anti-Synaptophysin (SP11) rabbit monoclonal antibody (1:20; cat. no. 790-4407), CONFIRM anti-S100 (1:50; rabbit polyclonal; cat. no. 760-2523), mouse monoclonal β-catenin (1:50; cat. no. 224M-1; Sigma-Aldrich; Merck KGaA), E-cadherin mouse monoclonal (1:50; cat. no. 790-4497; Ventana Medical Systems, Inc.) and mouse monoclonal anti-Ki-67 (1:20; cat. no. KI67-MM1-L-CE; Leica Microsystems, Inc.) antibodies were used for immunohistochemistry. Following inactivation of the endogenous peroxidase using a UV-inhibitor for 4 min at 37˚C, the primary antibody was added for 16 min at 37˚C, followed by the respective anti-mouse or anti-rabbit secondary antibody application of HRP Universal Multimer for 8 min, and detected using the ultraView Universal DAB Detection kit (cat. no. 760-500; Ventana Medical Systems, Inc.) for 38 min. Slides were counterstained at 25˚C with hematoxylin for 8 min and bluing reagent for 4 min before mounting with cover slips. Following staining, images were captured on Nikon Eclipse Ci series Upright Light-microscope using a NIKON Digital Microscope Camera-DS-Ri1, with NIS Elements imaging software (version 4.0) from Nikon Corporation. Appropriate positive controls for all of the studied antibodies were used.

*DNA isolation and NGS analysis on Ion Proton*. DNA isolation was performed by Qiagen FFPE kits (Qiagen Inc.). Briefly, five finely cut 5-10 $\mu$m of formalin-fixed paraffin-embedded sections were deparaffinized using xylene, cleaned with ethanol to remove xylene, and the pellet was dried at 65˚C for 5 min. The pellets were resuspended in buffer ATL, treated with proteinase K and the later steps were carried out according to the user manuals. DNA (10 ng) was used for NGS analysis, and DNA was sequenced using Ion PI v3 chip (Thermo Fisher Scientific, Inc.) on Ion Proton instrument (22). Libraries were prepared using Ion AmpliSeq comprehensive cancer panel (Thermo Fisher Scientific, Inc.) primer pools. Ion AmpliSeq 2.0 library kit, and Ion PI Hi-Q OT2 200 kit, (Thermo Fisher Scientific, Inc.) was used for libraries and templates preparation, respectively. Sequencing was done using Ion PI Hi-Q Sequencing 200 kit (Thermo Fisher Scientific, Inc.). Libraries were tagged with Ion Express barcodes (Thermo Fisher Scientific, Inc.). Following DNA sequencing, amplicon sequences were aligned to the human reference genome GRCh37 (hg19) in the target region of comprehensive cancer panel gens by using the Torrent Suite software (version 5.10.1.0; Thermo Fisher Scientific, Inc.). Variant call format (vcf) file was generated by running the Torrent Variant Caller Plugin v5.2, (Thermo Fisher Scientific, Inc.). Low quality reads filtering and variant annotations were done on Ion Reporter software (version 5.10.2.0; Thermo Fisher Scientific, Inc.) for the annotation. The 'vcf' files data were also analyzed using Advaita Bioinformatics' iVariantGuide (http://www.advaitabio.com/ivariantguide) to determine for significant variants, associated genes, predicted impacts and clinical significance.

More details of data analysis and annotation sources included in Ion Reporter software (Ion Reporter Software 5.6

Publication Number MAN0017204) were obtained, including variant types, single nucleotide polymorphisms (SNP), insertions and deletions (Indel), P-value, PolyPhen-2 and coverage analysis. The coverage parameters were used to avoid false-positive calls that could result from sequencing coverage not wide enough to provide a correct genotype. Allele coverage corresponded to the number of reads supporting the called allele, and the frequency of the allele observed was annotated as frequency from the raw data. The P-value was the probability that the variant call made was correct. P-values closer to 0.0 indicated high confidence in the variant call. P-values closer to 1.0 represent indicated low confidence in the variant call. The P-value corresponded to a logarithmic transformation of the Phred quality score value made by the Variant caller plugin in Torrent Suite software (version 5.10.1.0; Thermo Fisher Scientific, Inc.) using an Ion Proton machine. For example, a variant caller quality score of 20 is associated with a P-value of 0.01, and a variant caller quality score of 30 is associated with a P-value of 0.001. Tumor variants with no coverage or low coverage were designated as non-confident, and the non-confident variants were not assigned a P-value. These workflows do analysis reads of a tumor sample and reads against the related reference sequence. These workflows allowed a statistical evaluation of the likelihood that the tumor allele may not be present in the normal sample, and determine a P-value that represented the statistical confidence of this call. True mutations have been considered based upon Phred quality score (i.e., -log10 of the probability that the alternative call is wrong), which was above 20, and mutation with P-value <0.05 were considered to be significant. The PolyPhen (Polymorphism Phenotyping; version 2.0; http://genetics.bwh. harvard.edu/pph2) score predicted the possible impact of an amino acid substitution on the structure and function of a human protein (23). This score represented the probability of a substitution to create damage. The PolyPhen score ranged from 0.0 (tolerated damage) to 1.0 (deleterious damage).

**Results**

*Clinical presentation and radiology*. A 3 years old girl was presented with acute subdural hemorrhage (non-traumatic) with fever, loss of conscious and poor oral intake. The child has a long head with a circumference of 53 cm. The patient underwent right frontoparietal craniotomy, tumor excision, admitted into pediatric intensive care unit (PICU) where she was extubated and into neurosurgery ward. The biopsy specimen obtained was of tan polypoid formation that consisted in multiple tissue fragments of rubbery consistency and measuring 5x4x0.5 cm. The proteins concentration in CSF was high (1,213.9 mg/dl; normal range, 15-45 mg/dl), the neutrophil count was low and monocyte count was high. CSF culture showed no growth, ruling out the possibility of infection. Partial thromboplastin time and international normalized ratio were normal (13.1 sec and 1.01, respectively). Blood chemistry and complete blood count results were normal. Routine radiological and immune-histological investigations were performed.

The pre-operative computed tomography (CT) examination revealed a fairly large solid lobulated well-demarcated intraventricular mass that was isodense to
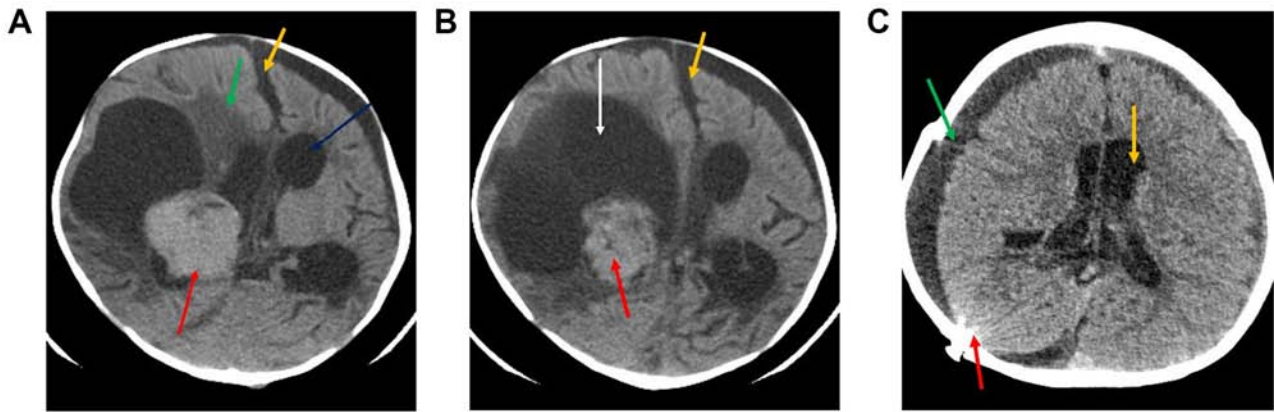
Figure 1. (A and B) Preoperative CT scan with contrast. The CT scans revealed a fairly large solid lobulated well-demarcated intraventricular mass lesion displaying homogenous contrast enhancement adjacent to the right lateral ventricle. This lesion measured ~3.7x4.3 cm and presented a large eccentric cystic component (white arrow), irregular margins, associated mass effect, midline shift (yellow arrows), perilesional edema (green arrow) and moderate supra-tentorial hydrocephalus (blue arrow). (C) Post-operative CT scan without contrast. Evidence of right craniectomy and extra-axial fluid collection (green arrow). No evidence of mass lesion was seen. Mild supratentorial hydrocephalus was observed (yellow arrow), as well as evidence of shunt (red arrow). CT, computed tomography.
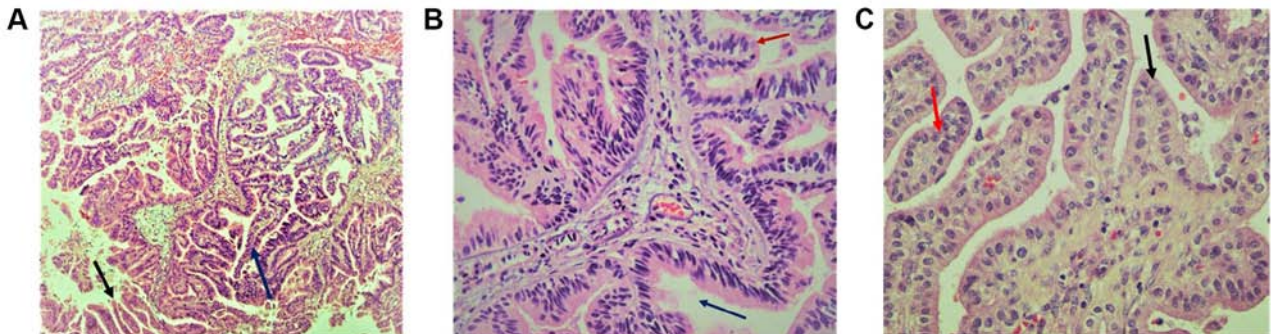


Figure 2. H&E staining showed proliferation of cuboidal cells arranged in a distinct papillary growth pattern and mitotic figures. (A) Delicate papillary fronds presented fibrovascular papillae lined by monomorphic epithelial cells and displaying papillae lined by layers of cubo-columnar cells (magnification, 10x). Arrows indicated as follows: Blue arrow, choroid plexus; red arrow, palisading pattern of cells. (B) H&E slide isomorphic nuclei and moderate amount of cytoplasm presented increased mitotic activity and architectural complexity (magnification, 20x). Arrows indicated Red intraventricular space. (C) In a-CPP with typical papillary arrangements (blue arrow), a single layer of cuboidal or columnar epithelium in a papillary configuration covering a fibrovascular core and mitotic cells were observed (magnification, 40x; Red arrow). H&E, hematoxylin and eosin.

mildly hyperdense (red arrow; Fig. 1A and B). This lesion presented homogenous contrast enhancement, which was adjacent to the right lateral ventricle (Fig. 1A). This lesion measured ~3.7x4.3 cm, exhibited a large eccentric cystic component (orange arrow), and possessed irregular or invasive margins with associated mass effect. midline shift (yellow arrow), perilesional oedema (green arrow) and moderate supra-tentorial hydrocephalus (white arrow) is also noted (A and B). Post-operative CT (Fig. 1C) revealed that, following right craniectomy and extra-axial fluid collection (green arrow), no evidence of mass lesion could be seen. Mild supratentorial hydrocephalus was observed (yellow arrow), as well as evidence of radiopaque shunt marker (red arrow) in the right parieto-occipital location.

*Histopathology and immunohistochemistry.* Histopathology of the papillary lesions stained with H&E is presented in Fig. 2. Tumor examination revealed a fibrovascular papil-lary projection of choroid plexus that was lined by columnar epithelium with crowding, elongation and stratification, displaying papillae lined by layers of cubo-columnar cells having isomorphic nuclei and moderate amount of cytoplasm delicate papillary fronds (Fig. 2A). In Fig. 2B, H&E stain revealed proliferation of cuboidal cells arranged in a distinct papillary growth pattern, mitotic figures, increased mitotic activity and architectural complexity. Furthermore, cells had increased nucleo-cytoplasmic ratio and increased mitosis, and the mitotic index was >2 mitoses/10 high-power fields (HPF). H&E slide with isomorphic nuclei and moderate amount of cytoplasm presented increased mitotic activity and architec-tural complexity, typical papillary arrangements, featuring a single layer of cuboidal or columnar epithelium in a papillary configuration covering a fibrovascular core and mitotic cells (Fig. 2C). Areas of cribriform projections and focal solid growth patterns were also seen (Fig. 2C). Immunostaining for S-100, Ki-67 and synaptophysin are presented in Fig. 3. Ki-67 and S-100 were strongly positive (Fig. 3A and B), and synaptophysin staining was focally positive (Fig. 3C). Ki-67 proliferation index was ≥85.0%. Immunohistochemistry for E-cadherin and β-catenin is presented in Fig. 4. The results
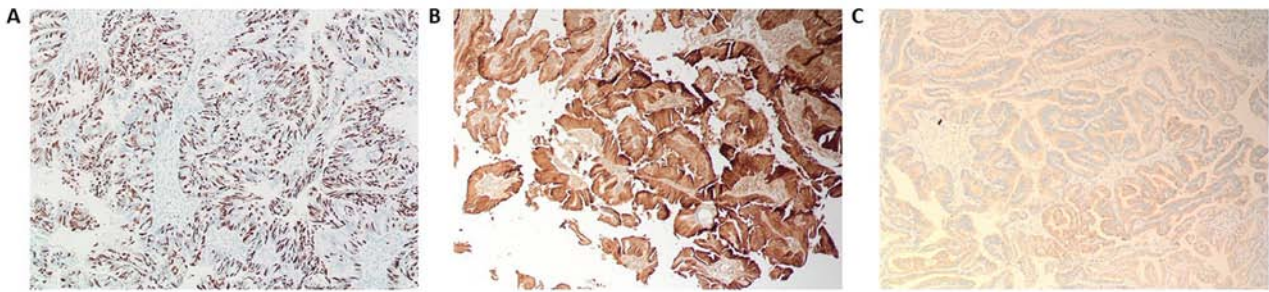
Figure 3. (A) Immunohistochemistry staining was strongly positive for Ki-67 in atypical CPP (magnification, 10x). (B) Microphotograph demonstrated a strong cytoplasmic immunopositivity for S-100 in the fibrovascular papillae lined by monomorphic epithelial cells (magnification, 10x). (C) Immunohistochemistry staining for synaptophysin was focally positive (magnification, 10x).
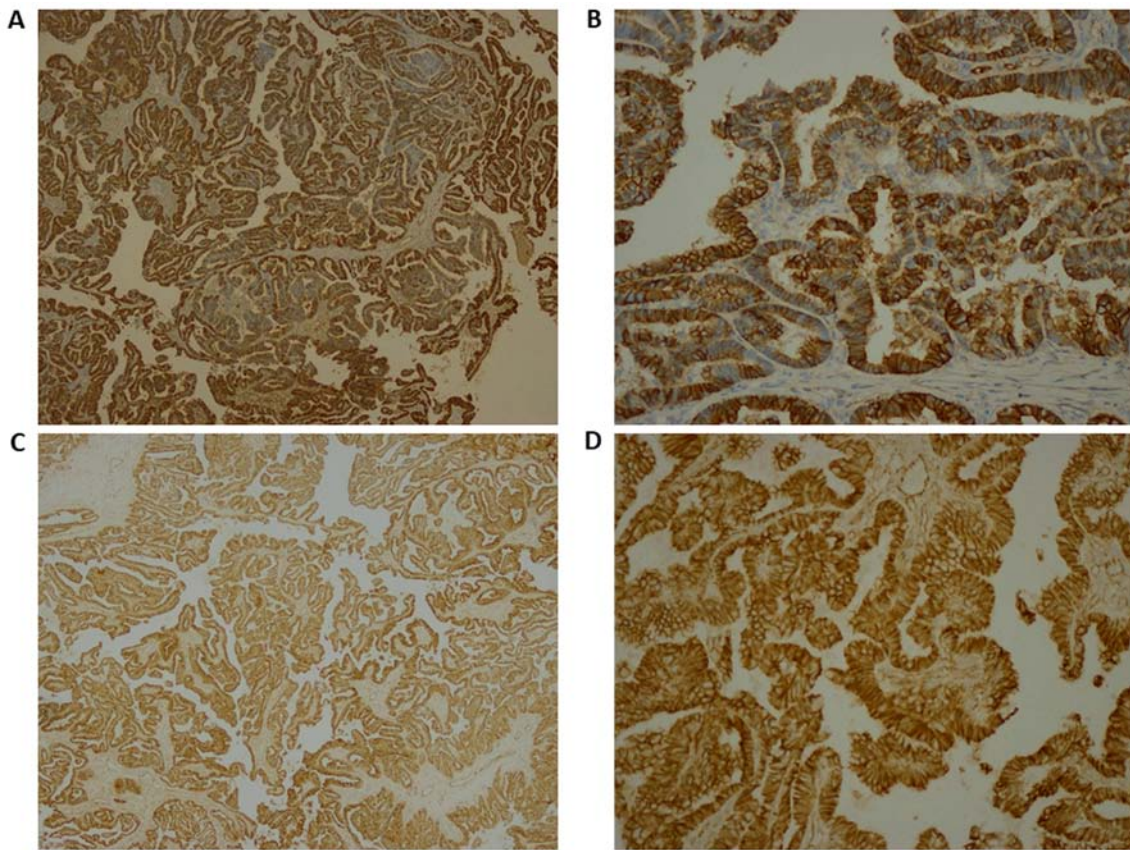


Figure 4. (A and B) Immunohistochemistry staining was strongly positive for E-Cadherin (magnifications, 4 and 20x, respectively) and for (C and D) β-catenin (magnifications, 4 and 20x, respectively).

revealed that membranes were positively stained for E-cadherin (Fig. 4A, magnification x4; Fig. 4B, magnification 20x) and β-catenin (Fig. 4C, magnification 4x; Fig. 4D, magnification 20x). As presented in Figs. S1 and S2, immunohistochemical staining for glial fibrillary acidic protein (GFAP), epithelial membrane antigen (EMA), vimentin, thyroid transcription factor 1, (TTF-1), P53, CK-7, and epidermal growth factor receptor (EGFR) were negative in this a-CPP tumor. The positive controls for these antibodies are shown in supplementary Fig. S3. The control tissues used for staining was astrocytoma for GFAP and P53, lung adenocarcinoma for CK7, papillary thyroid carcinoma for EGFR and TTF1, myxopapillary ependymoma for EMA and inflammatory mesenchymal tissue for vimentin staining.

*NGS data analysis variant identification and variant statistics.* Alignment analysis of the target regions (CCP. 20170413. designed) to the reference genome (Human genome build 19 of hg 19) and sample coverage overview was performed by the Ion Torrent Suite software v4.4.2 (Fig. 5). Amongst the 9,064,980 reads that were generated for this sample by Ion PI chip, 83.30% reads were on target, with an average base coverage depth of 459x and an uniformity of base coverage of 85.58%. Amplicon and target base read coverages of sequencing demonstrated that out of 16,000 amplicons, 15,992 amplicons were sequenced with Ion AmpliSeq comprehensive cancer panel primer pool (Table SI). The 1, 20, 100 and 500x target base coverage were 99.66, 96.55, 84.35 and 32.99%, respectively. In addition, the percent end-to-end reads of
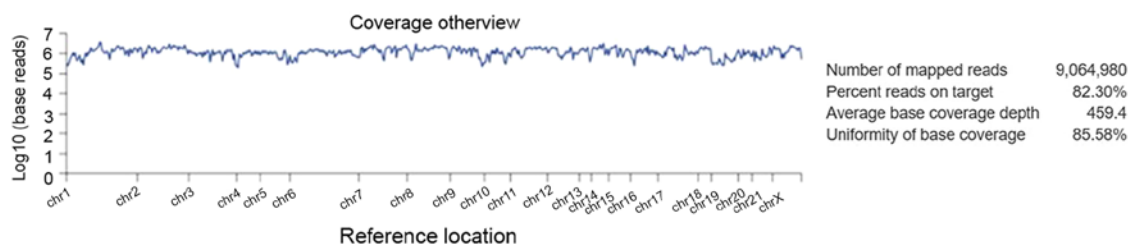
Figure 5. Alignment analysis of the target regions (CCP. 20170413.designed) to the reference genome (Human genome build 19 of Hg 19) and sample coverage overview as performed by the Ion Torrent Suite software v4.4.2 for Ion Proton sequencing.
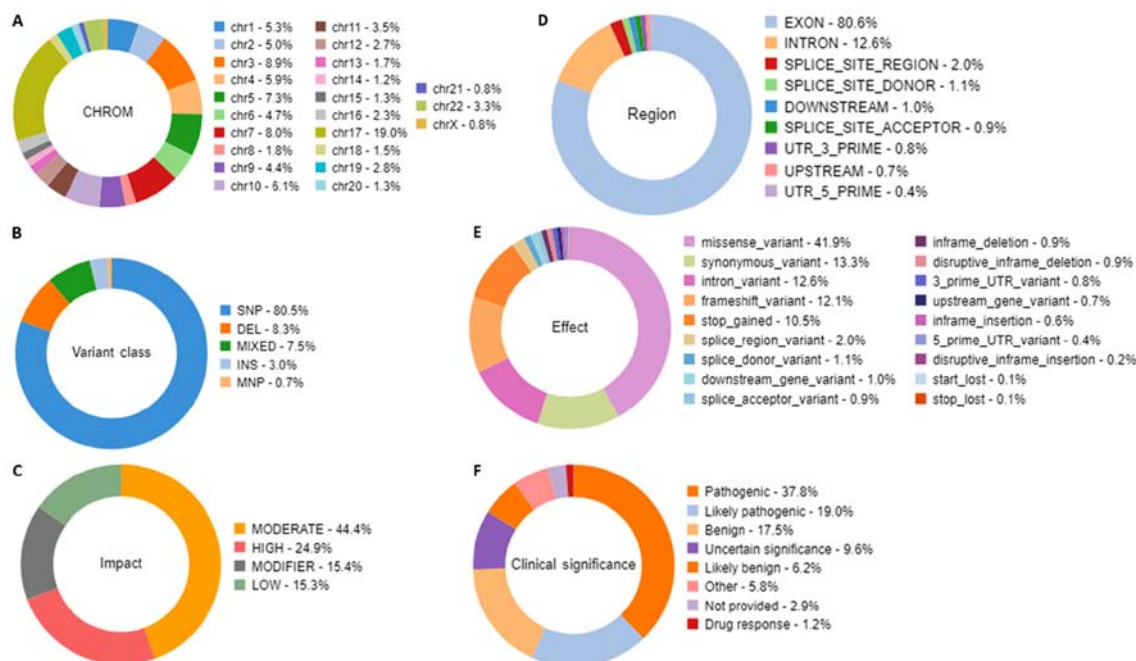


Figure 6. Statistical analysis distribution of the variants that passed through the filters. The filtration presented characteristics, including the relative number of variants located on each chromosome, the variant class, the substitution types, the insertion and deletion lengths, the variant effect that gives the changes occurring on the transcript, the genomic regions impacted by the variant, and the functional consequences of each variant on the interpretation of the score severity and on the impact to predict the severity of the disease. Doughnut charts in panels presented variants that had passed for each individual filter for (A) Chromosomal distribution, (B) Variant class, (C) Variant impact on the protein function, (D) Region in the gene, (E) Variant effect on the protein structure, and (F) Clinical significance of the variants annotated from the ClinVar database.

amplicons were 92.13% (Table SI). Initial analysis by Advaita's i-variant software demonstrated that 100% (3,650) variants passed all filters. The variants statistics distributions according to various filters, including chromosomal distribution, region in the gene, variant class, effect of variant on protein, variant impact and clinical significance are presented in Fig. 6. The chart from panel (A) represents the relative number of variants located on each chromosome. The results demonstrated that chromosome 17 possessed the highest variants (19%) whereas chromosome 21 and X chromosome had the least variants (0.8%). Panel (B) demonstrated that variant class represented SNPs at 80.5%, whereas deletions and insertions represented 8.3 and 3%, respectively. In panel C, variants passed through the variant impact filter, which gives a prediction of the disease severity, and the results revealed that 24.9% were of high impact whereas 44.4% variants had moderate impact on the protein structure and function. Furthermore, 80.6% were exonic, 12.6% were intronic and 2% were splice site variants (panel D). In addition, 41.9% were missense variants, 13.3%

were synonymous variants and 12.6% were intronic variants (panel E). Clinical significance represents variants that are associated with clinical outcomes, including susceptibility to diseases or response to drugs. By applying the clinical significance filter, the results revealed that 17.5% were benign variants and 37.8% were pathogenic variants (panel F).

The summary of all novel missense mutations found in CPP tumour are presented in Table I. In this a-CPP tumour, NGS data analysis identified 12 novel missense mutations by Ion Proton. The gene mutations detected were as follows: A missense mutation c.5808A>T p. (Leu1936Phe) on exon 39 of the ATM gene; a c.4214C>A p. (Pro1405His) mutation on exon 25 of NOTCH1 gene; a c.2439A>T p. (Gln813His) mutation on exon 21 of SKT36 gene; and a c.2026A>G p. (Arg676Gly) on exon 12 of MAGI1 gene. No exonic mutation in SMARCB1 was found in this tumor; however, one missense mutation c.2729C>T p. (T910M) was detected in SMARCA4 gene. Furthermore, novel missense variants were identified in exon 86 of DST, in exon 8 of RECQL4, in exon 15 of NUMA1, in

Table I. Novel missense variants observed in atypical choroid plexus papilloma tumor.

| Chromosomal position | Ref | Observed allele | Frequency (%) | Gene | Coding | AA change | Phred quality score | Exon |
|---|---|---|---|---|---|---|---|---|
| chr9:139400134 | G | T | 15 | NOTCH1 | c.4214C>A | p. (Pro1405His) | 47.805 | 25 |
| chr11:108180932 | A | T | 3.45 | ATM | c.5808A>T | p. (Leu1936Phe) | 23.909 | 39 |
| chr2:219559286 | A | T | 25 | STK36 | c.2439A>T | p. Gln813His | 36.7001 | 21 |
| chr3:65415336 | T | C | 19.89 | MAGI1 | c.2026A>G | p. Arg676Gly | 625.727 | 12 |
| chr6:56341107 | T | A | 28.71 | DST | c.15347A>T | p. Gln5116Leu | 423.313 | 86 |
| chr8:145740605 | T | G | 11.63 | RECQL4 | c.1412A>C | p. Gln471Pro | 44.974 | 8 |
| chr11:71724390 | G | C | 9.35 | NUMA1 | c.4159C>G | p. Gln1387Glu | 38.5888 | 15 |
| chr15:39884882 | G | T | 80.65 | THBS1 | c.2646G>T | p. Gln882His | 635.503 | 17 |
| chr16:15844106 | C | T | 11.11 | MYH11 | c.1968G>A | p. Met656Ile | 25.4788 | 17 |
| chr18:56383196 | T | G | 4.94 | MALT1 | c.1015T>G | p. Leu339Val | 20.2404 | 9 |
| chr18:59221876 | G | A | 10.99 | CDH20 | c.2354G>A | p. Arg785Gln | 109.339 | 12 |
| chr19:11132513 | C | T | 0.75 | SMARCA4 | c.2729C>T | p. T910M | 22.6552 | 19 |

AA, amino acid.

Table II. Known missense variants observed in atypical choroid plexus papilloma tumor.

| Chromosomal position | Ref | Observed allele | Frequency (%) | Gene | Coding | AA change | Phred quality score | Variant ID | Exon |
|---|---|---|---|---|---|---|---|---|---|
| chr11:108183167 | A | G | 99.22 | ATM | c.5948A>G | p. (Asn1983Ser) | 1954.99 | COSM4590264 | 40 |
| chr3:128202753 | G | A | 92.31 | GATA2 | c.967C>T | p. His323Tyr | 813.943 | COSM6854635 | 4 |
| chr4:1808286 | G | A | 93.54 | FGFR3 | c.2044G>A | p. Val682Ile | 4487.31 | COSM6854620 | 16 |
| chrX:53223568 | G | A | 7.49 | KDM5C | c.3791C>T | p. Ala1264Val | 39.1666 | COSM6978062 | 23 |
| chr2:29416572 | T | C | 100 | ALK | c.4381A>G | p. Ile1461Val | 9246.4 | rs1670283 | 29 |
| chr5:112179149 | T | A | 19.78 | APC | c.7858T>A | p. Phe2620Ile | 233.547 | rs587781816 | 16 |
| chr7:55259448 | C | T | 0.84 | EGFR | c.2506C>T | p. R836C | 27.6404 | COSM28604 | 21 |
| chr7:55259493 | G | A | 0.79 | EGFR | c.2551G>A | p. V851I | 30.2797 | COSM12727 | 21 |
| chr7:55259511 | G | A | 1.27 | EGFR | c.2569G>A | p. G857R | 21.9957 | COSM12764 | 21 |
| chr7:55270310 | C | T | 43.99 | EGFR | c.3263C>T | p. Pro1088Leu | 1215.33 | rs771418435 | 27 |

AA, amino acid.

exon 17 of THBS1, in exon 17 of MYH11, in exon 9 of MALT1 and in exon 12 of CDH20 (Table I). In addition, a novel mutation was identified in the exon 39 of ATM gene locus chr11:108180932. This mutation c.5808A>T (p. Leu1936Phe) was a missense mutation, and the coding at this position changed the nucleotide sequence from TTA to TTT. The allele ratios for A and T were 0.9655 and 0.0345, respectively, and the frequency of this mutation (A>T) was 3.45%. For this mutation, the coverage of this variant was 69x, the P-value was 0.00407 and the Phred quality score was 23.909 (Table SII). For each target, frequency, allele coverage, allele ratio, P-value Phred scores and PolyPhen scores were determined for these novel mutations (Tables II and SII). The P-value and Phred quality score were significantly high for all mutations, as revealed by the Ion Reporter analysis reads of a tumor sample and reads against the associated reference sequence. Only

one novel missense mutation, the c.2646G>T p. (Gln882His) mutation on gene THBS1, had a frequency of 80.65% and a Phred quality score of 635.503, which indicated that this was a germline mutation (Table I). The PolyPhen score of the six variants viz. DST, RECQL4, NUMA1, THBS1, MYHI1 and SMARCA4 were high, which suggested that these variants may be pathogenic variants, whereas NOTCH1 had a PolyPhen score of 0.429, which indicated that it may be pathogenic. Other variants had low PolyPhen scores (Table SII).

In this tumor, 10 missense mutations identified (Table II) by Ion Proton have been previously reported in COSMIC(https://cancer.sanger.ac.uk/cosmic), EXAC browser, (http://exac.broadinstitute.org/) and dbSNP databases (https://www.ncbi.nlm.nih.gov/snp/). As described in Table II, the four known missense mutations identified in this case were in exon 16 of APC (c.7858T>A), in exon 16 of FGFR3

(c.2044G>A), in exon 40 of ATM (c.5948A>G) in exon 29 of ALK (c.4381A>G), in exon 23 of KDM5C (c.3791C>T) and in exon 4 of GATA2 (c.967C>T). Three known mutations were detected (c.2506C>T, c.2551G>A and c.2569G>A) in exon 21 of EGFR, and, one mutation (c.3263C>T) was also found in exon 27 of EGFR. The quality statistics for these mutations are presented in Table SIII. Among these previously reported missense variants, the ATM, GATA2, FGFR3 and ALK (rs1670283) variants have a frequency of 99.22, 92.31, 93.54 and 100.00% respectively, suggesting that they may be germline mutations (24,25). All other variants had low frequencies suggesting those are somatic mutations (Table II). The PolyPhen scores of three variants viz. of GATA2 (c.967C>T), FGFR3 (c.2044G>A), KDM5C (c.3791C>T), and of three variants of EGFR (c.2506C>T; c.2551G>A; and c.2569G>A) were high, which suggested that they were pathogenic variants; however another EGFR variant (c.3263C>T) had a low score (Table SIII).

Table III exhibits the insertions, deletions and nonsense variants that were identified in the a-CPP tumor tissue. The two novel insertions found were as follows: The viz. c.1056_1057insG. andc.1056_1057insA in PARP1 gene, and the c.21904_21905insG in SYNE1 gene. Both caused frameshift, and the deletion variant in NOTCH1 c.4732_4734delGTG p. (Val1578delVal) caused a frameshift in reading frame. Two novel nonsense mutations were also identified in MET gene (c.525T>A; p. Cys175Ter) and in RNF213 gene (c.6967C>T; p. Gln2323Ter). Quality statistics of these variants are presented in Table SIV and comprised allele coverage, allele ratio, P-value, Phred quality score, sequencing coverage and alleles frequency. The P-value and Phred quality score were significantly high for all the variants as revealed from the Ion Reporter analysis reads of a tumor sample and reads against the associated reference sequence. However, the allele frequency of PARP1 was low whereas other variants had higher frequencies (Table SIV), including SYNE1 insertion mutation (p. Phe7302fs) that had a frequency of 100%, which indicated they may be germline mutations.

The present study also identified 15 novel synonymous mutations in the a-CPP tumor. They were located in exons 11, 7, 21, 14, 12, 16, 13, 10, 24, 46, 19, 21, 1, 4 and 4 of the genes viz. ABL1, AKT1, PIK3CA, FGFR3, PDGFRA, APC, RET, SMAD4, NOTCH2, IGF2R, ADGRA2, PRKDC, PAX5, TET1 and IDH2, respectively (Table IV). As presented in Table IV, FGFR3, PDGFRA, RET, IGF2R, ADGRA2, PRKDC and PAX5 synonymous variants had high frequencies, whereas other synonymous variants were low frequency variants. The coverage details of these synonymous mutations are described in Table SV. In Table V the novel intronic variants identified in the a-CPP tumor tissue are listed. The results demonstrated that amongst the 13 novel intronic variants identified in the present case, the intronic SNPs were in genes viz. PMS1, FGFR1, ERBB4, RET, FGFR3, SMARCB1, PAX3, SDHA, LIFR, PDGFRB, MAP3K7, PRKDC and AKT2. In addition, a splice site mutation at acceptor site (c.132+1G>C) in PMS1 gene, a variant in 3'-UTR of WT1 gene, and a SNV in 5'-UTR of BRD3 gene were also identified (Table V). Quality statistics of these novel intronic variants found in a-CPP patient are presented in Table SVI and comprised allele coverage, allele

Table III. Novel and known frameshift and nonsense variants observed in atypical choroid plexus papilloma tumor.

| Chromosomal position | Ref | Observed allele | Frequency (%) | Gene | Coding | AA change | Phred quality score | Exon |
|---|---|---|---|---|---|---|---|---|
| chr9:139399408 | GCACCACCACCA | GCACCACCA | 0.93 | NOTCH1 | c.4732_4734delGTG | p. (Val1578delVal) | 112.162 | 26 |
| chr1:226570839 | G | GC, GT | GC=53.44, T=46.56 | PARP1 | c.1056_1057insG, c.1056_1057insA | p. Gln353fs, p. Gln353fs | 8,388.56 | 11 |
| chr6:152540277 | A | AC | 100 | SYNE1 | c.21904_21905insG | p. Phe7302fs | 3,142.24 | 7 |
| chr7:116339663 | T | A | 8.26 | MET | c.525T>A | p. Cys175Ter | 197.511 | 21 |
| chr17:78319102 | C | T | 12.78 | RNF213 | c.6967C>T | p. Gln2323Ter | 247.344 | 14 |

AA, amino acid.

Table IV. Novel synonymous variants observed in atypical choroid plexus papilloma tumor.

| Chromosomal position | Ref | Observed allele | Frequency (%) | Gene | Coding | AA change | Phred quality score | Exon |
|---|---|---|---|---|---|---|---|---|
| chr3:178952089 | T | C | 4.96 | PIK3CA | c.3144T>C | p. (His1048His) | 99.3152 | 21 |
| chr4:1807894 | G | A | 100 | FGFR3 | c.1953G>A | p. (Thr651Thr) | 31973.5 | 14 |
| chr4:55141055 | A | G | 100 | PDGFRA | c.1701A>G | p. (Pro567Pro) | 31992 | 12 |
| chr10:43613843 | G | T | 100 | RET | c.2307G>T | p. (Leu769Leu) | 31955.9 | 13 |
| chr1:120469164 | C | A | 3.75 | NOTCH2 | c.3963G>T | p. (Val1321Val) | 25.14 | 24 |
| chr6:160523656 | G | A | 84.72 | IGF2R | c.6948G>A | p. (Ala2316Ala) | 1694.61 | 46 |
| chr8:37698673 | C | G | 60.44 | ADGRA2 | c.2817C>G | p. (Thr3939Thr) | 1510.27 | 19 |
| chr8:48839854 | T | C | 47.76 | PRKDC | c.2319A>G | p. (Leu773Leu) | 8421.16 | 21 |
| chr9:37033987 | C | T | 50.04 | PAX5 | c.42G>A | p. (Arg15Arg) | 6613.8 | 1 |
| chr10:70406386 | C | A | 17.91 | TET1 | c.3900C>A | p. (Thr1300Thr) | 200.101 | 4 |
| chr15:90631834 | G | A | 6.04 | IDH2 | c.519C>T | p. (His173His) | 33.0969 | 4 |

AA, amino acid.

Table V. Novel intronic variants observed in atypical choroid plexus papilloma tumor.

| Chromosomal position | Ref | Observed allele | Frequency (%) | Gene | Coding | Phred quality score |
|---|---|---|---|---|---|---|
| chr2:212522461 | A | C | 46.69 | ERBB4 | c.1946+18T>G | 1,140.64 |
| chr10:43613960 | C | T | 6.34 | RET | c.2392+32C>T | 22.0765 |
| chr8:38272057 | A | C | 30.43 | FGFR1 | c.2141+20T>G | 45.0631 |
| chr4:1808524 | G | A | 7.47 | FGFR3 | c.2169-32G>A | 277.191 |
| chr2:190656668 | G | C | 7.65 | PMS1[a] | c.132+1G>C | 221.546 |
| chr2:190717340 | A | C | C=6.77 | PMS1 | c.700-41A>C | 53.9539 |
| chr2:223158437 | CTC | C | 14.29 | PAX3 | c.586+449GAG>G | 94.7574 |
| chr5:233504 | T | C | 5.56 | SDHA | c.896-88T>C | 24.9682 |
| chr5:38493661 | T | A | 28.86 | LIFR | c.2065+47A>T | 1,786.08 |
| chr5:149499530 | A | T | A=24.24, | PDGFRB | c.2698+45T>A | 207.989 |
| chr6:91228938 | AGAA | A | 6.35 | MAP3K7 | c.1524+39TTCT>T | 24.0052 |
| chr8:48847670 | CA | AC | 4.79 | PRKDC | c.1448-52TG>GT | 47.8405 |
| chr9:136918606 | G | A | 19.05 | BRD3, LOC100130548[b] | c.-7C>T | 20.7564 |
| chr11:32410514 | T | C | 19.58 | WT1[c] | c.1644A>G | 353.703 |
| chr19:40744051 | C | A | 8.16 | AKT2 | c.709-53G>T | 38.5654 |
| chr22:24167632 | T | C | 27.78 | SMARCB1 | c.986+30T>C | 83.9641 |

[a]splicesite_3; [b]5'-utr; [c]3'-utr. AA, amino acid.

ratio, P-value, coverage and alleles frequencies. P-values as presented in Table SVI and Phred quality scores as presented in Table V were significantly higher for these novel intronic variants.

## Discussion

The a-CPP grade II tumor is situated between the CPP and CPC tumors (11). A-CPP tumors were previously considered to be a separate pathologic subgroup that exhibits an intermediate degree of mitotic activity and overall survival rate. The intermediate position of a-CPP between CPP and CPC was supported by the clinical data, such as the presence of metastases at diagnosis, event-free survival rates, and increases in Ki-67 proliferation marker and the p53 tumor suppressor protein across the three histological subtypes (from CPP to a-CPP and then CPC) (26). Histopathological examination of this tumor revealed increased mitotic index of 2 mitoses/10 HPF and cribriform morphology, which confirmed that, according to the diagnostic criteria of WHO classification of CNS tumors, the present case was an a-CPP (27). Extensive metastasis from CPPs can take place into the subarachnoid

space when the tumors are malignant (28). In low-grade CPP, the unique papillary configuration is a distinct feature, whereas in CPC the papillary features are unclear and this ill-defined growth pattern sometimes makes the diagnosis challenging (29). The fibrovascular papillary projections of CPP are lined by cuboidal to columnar epithelium compared with normal choroid plexus tissue, which has orderly cobblestone appearance (1,5). CPP tumours commonly exhibit higher nuclear-to-cytoplasmic ratio and nuclear hyperchromasia. This was the first case of a-CPP reported in Saudi Arabia. However, a case of CPP was reported by Jamjoom *et al* (30).

Most of the CPP cases have strong immunoreactivity to S-100 protein, whereas glial fibrillary acidic protein (GFAP) are expressed weakly and only focally in a few tumors (31). In the present study, no EMA staining was observed, although it has been reported to be commonly positive in CPP cases (32). In the present study, GFAP and EGFR staining was negative, whereas synaptophysin was focally positive. GFAP, synaptophysin, transthyretin and S100 protein stainings were reported to be more variable in CPP cases (33). However, pan-cytokeratin and vimentin are commonly positively expressed in CPP tumours (1,33). It has been reported that most CPPs express cytokeratins, vimentin and podoplanin, and are also usually positive for E-cadherin (4,34). The loss of E-cadherin expression would increase cell proliferation migration and invasion (35,36). Although E-cadherin is present on the basolateral surface of the majority of CPPs, decreased expression in atypical papillomas and CPCs has been reported; however, the present study demonstrated positive staining for E-cadherin (37,38).

The novelty of the mutations identified in the present study (Table I) were verified by COSMIC and ExAc databases. Several molecular pathways associated with CPC have been previously reported and allow distinction of CPC from CPTs (11,39,40). Mutations in TP53 were demonstrated to be associated with increased tumor aggressiveness and worsen survival outcome in CPCs; however, no mutation in TP53 was reported in a-CPP and it is in agreement with the results from the present study (11,39-41). No mutation profiling in CPP cases has been previously attempted by NGS methods; however, it was done in numerous types of brain tumor and used to distinguish these tumors from their mutational profiles (42,43). For example, the distinction between adamantinomatous craniopharyngiomas and papillary craniopharyngiomas was based upon the presence of mutations in the genes catenin-β 1 (CTNNB1) and B-Raf proto-oncogene, serine/threonine kinase following whole exome sequencing (44). To the best of our knowledge, mutations in the genes NOTCH1, ATM, STK36, MAGI1, GATA2, FGFR3, DST, RECQL4, NUMA1, THBS1, MYH11, MALT1, CDH20 and KDM5C have been reported in CPP tumors. STK36 is a serine/threonine protein kinase that serves a crucial role in the sonic hedgehog pathway by regulating the activity of the GLI transcription factors and that is essential for postnatal development, which may be mediated by CSF homeostatis or ciliary function regulation (45). Overproduction of CSF, growth retardation, hydrocephalus development and early mortality were reported in STK36 knockout mice (45). CSF overproduction also worsens the risk of developing hydrocephalus (6). The patient from the present study also presented hydrocephalous and CSF accumulation. This indicates that STK36 mutations may serve a crucial role in choroid plexus

tumor progression. However, further investigation is required to understand this phenomenon. Shajani-Yi *et al* (46) reported that 28% patients with glioblastoma present mutations in TP53, following NGS using Cancer HotSpot Pane, and also identified mutations in clinically actionable genes, including IDH1, IDH2, CDKN2A and PIK3CA (46). In the present study we have also found a known missense mutation in exon 5 of TP53, mutation in c.419C>T p. (T140I COSM43742), with a p. value of 0.05396, Phred quality score of 12.6795 and frequency of 1.36% (not shown in results). A missense mutation in the exon 10 of IDH2 was also observed in this tumor. This mutation in c.1261G>A (p. Gly421Ser COSM3420710) had a frequency of 5.06%, a P-value of 0.01377 and a Phred quality score 18.6103 (not shown in results). These two mutations have Phred score <20, and were subsequently not included in the analyses or Tables. In addition, the tumor from the present study presented a novel synonymous variant in IDH2. The a-CPP tumor assessed in the present study harbored mutations only in the EGFR, a driver gene for glioma, activation and autophosphorylation domains, whereas other driver genes for various gliomas, such as TP53, PTEN, NF1 and IDH1, did not have any mutations (47,48). The present study was the first to reveal a complete mutational profile of a-CPP tumor by NGS technology on an Ion Proton platform and using 409 tumor suppressor and oncogenes targeted for mutations. It has been reported that glioblastoma tumors frequently overexpress the mesenchymal-epithelial transition (MET) proto-oncogene, of which expression correlates with tumor grade. In addition, MET signaling confers resistance to radiotherapy, and various MET inhibition strategies are being developed to treat GBM tumors (49). A novel nonsense mutation c.525T>A p. (Cys175Ter) in a-CPP tumor was reported in the present study.

The present study identified a novel intronic variant in hSNF5/INI1 (SMARCB1) gene. No exonic mutation was found in SMARCB1; however, one missense mutation was detected in SMARCA4 gene. Hasselblatt *et al* (2011) reported that a nonsense mutation inactivates SMARCA4 in an atypical teratoid/rhabdoid tumor with intact SMARCB1 (INI1) expression (50). To the best of our knowledge, the present study is the first to report that SMARCA4 mutation is associated with a-CPP. For the first time in brain tumors, four missense variants in ATM, GATA2, FGFR3 and KDM5C and one deletion variant in NOTCH1 were identified in the present study. The ATM missense mutation [c.5948A>G; p. (Asn1983Ser)] identified in the present study was of germline origin, according to ClinVar database by 'Ambry Genetics' with the variation ID No. 140790. This mutation was also found in SNP database with rs # 659243, and in a patient with familial history gastrointestinal cancer; however, to the best of our knowledge, this mutation has not been reported in patients with brain cancer (24). This ATM mutation [c.5948A>G; p. (Asn1983Ser)] is adjacent to the Ser 1981 and Ser 1985, which is a part of the focal adhesion targeting (FAT) domain that is required for ATM autophosphorylation (51,52). However, this mutation was reported to be benign with a FATHMM prediction score 0.01 (53). The mutation reported in the a-CPP case from the present study in exon 16 of the FGFR3 gene [COSM6854620 c.2044G>A p. (Val682Ile)] had also been reported previously in large intestine (25), with a FATHMM prediction score of 0.97, which suggests that this mutation

might be pathogenic (25). However, this mutation has not yet been reported in brain tumors.

The formation of various types of tumor in humans is modulated by NOTCH signaling pathway, which has been reported to serve a crucial role in the development and formation of normal choroid plexus (54). Insertion of G and A in PARP1 gene (c.1056_1057insG and c.1056_1057insA) causes a frameshift in the reading frame and a termination at 35th coding position from this insertion. In addition, insertion of G (c.21904_21905insG) in PARP1 causes a frameshift in the reading frame and a termination codon at 3rd coding position from insertion (55). PARP enzymes are involved in DNA damage repair (56). Mutations in SYNE1 (ARCA1) gene are known to cause autosomal recessive cerebellar ataxia type-1 (57), and patients with CPP are known to have symptoms of ataxia (5). Previous studies reported that SYNE1 and STK36 mutations are present in GBM cases (58). In addition, deletion variant in NOTCH1 [c.4732_4734delGTG p. (Val1578delVal)], which causes a frameshift in reading frame, was also observed in hematopoietic and lymphoid tissues, but this variant has not previously reported in GBM (59). Mutations in NOTCH1 are associated with altered drug sensitivity, such as to tyrosine kinase inhibitors (60). Frameshift-deletion in exon 26 of NOTCH1 has been reported in hematopoietic and lymphoid skin, salivary gland and thymus (61). KDM5C, also known as 'Jumonji. AT-rich interactive domain 1c' JARID1C, codes for a histone demethylase, and mutations in this gene are associated with mental retardation and microcephaly (62). This suggests that alteration in chromatin remodeling might serves a role in CPP. It is therefore crucial to further investigate choroid plexus tumor to better understand the role of chromatin remodeling, since this type of tumor exhibits mutations in enzymes responsible for chromatin remodeling, including PARP, SMARCA4 and ATM. A mutation in GATA2 gene [c.967C>T p. (His323Tyr)] has been previously identified in large intestine with a FATHMM prediction score of 1.00 (25). To the best of our knowledge, the missense mutation detected in the GATA2 gene in the present study has not yet been reported in GBM tumors. GATA2 is a hematopoietic factor that has been implicated in hematopoietic malignancies, and this transcription factor has been implicated in prostate tumorigenesis (63,64).

ATM kinase is an important tumor suppressor, and its activation causes the phosphorylation of numerous targets, including proteins involved in cell cycle arrest, DNA repair and apoptosis (65). Blake *et al* (66) have demonstrated that inactivation of the ATMIN/ATM pathway protects against glioblastoma pathogenesis. Eich *et al* (67) revealed that ATM and ATR inhibition sensitizes cancer cells to temozolomide (TMZ) and to other anticancer compounds. In addition, several studies also reported that ATM- and ATR (ataxia telangiectasia and Rad3 related)-mutated cells are sensitive to TMZ mediated cytotoxicity (68), Inhibition of ATM-AMPK enhances TMZ-induced cytotoxicity in inherently TMZ-sensitive glioma cells, and ATM kinase inhibition also sensitizes p53 mutant glioma cells to ionizing radiation (69,70). The novel mutation revealed in the present study was located on chromosome 11, in the exon 39 of ATM gene. In addition, amongst patients with prostate cancer in AT heterozygotes, a higher proportion ATM exon 39 polymorphism (G5557A) was reported (71).

Copy number analysis by molecular inversion probe method revealed focal chromosomal gains in the region of chromosome 11, which is where ATM gene locus is present (31).

Ion AmpliSeq comprehensive cancer panel consists of 16,000 primers supplied in 4 tubes (aliquots), which targets 409 genes. This panel targets the exons of numerous tumor suppressor genes and oncogenes that are frequently mutated in various types of cancer. The mutations detected in the present study with the Ion Proton system presented high accuracy and high depth of coverage, which allowed to reliably detect low frequency mutations with high confidence. Individual allele coverage for this novel ATM mutation A>T are in forward strands, the sequencing reads for the A allele are 1,026 and 904, respectively, and for the T allele, the sequencing reads are 45 and 24 respectively. This variant coverage was 1999, mutation frequency was 3.45%, allele frequency was 0.034517 and P-value was 0.00407. Instead of using whole exome sequencing, cancer panels analysis also became a common practice on Ion Proton. A previous study analyzed circulating tumor DNA in non-small cell lung cancer by Ion Proton (22). This instrument offers the advantage of pooling more samples using the barcodes, which is what the authors of the aforementioned study did by using Ion AmpliSeq Colon and Lung Cancer Research Panel v2 on Ion Proton. Pooled samples sequencing using Ion PI chip enables a highest throughput up to 15 Gb data, with >60-80 million reads passing filter.

It is crucial to obtain well-calibrated quality scores, since SNP and genotype calling at a specific position in the genome depends on the base calls and the per-base quality scores of the reads overlapping the position. Coverage values represent the read depth (DP), which represents the number of reads passing quality control that are used to calculate the genotype at a specific site and in a specific sample with higher values for DP, generally leading to more accurate genotype calls (72). In the present study, the Phred quality score of the novel ATM variant was 23.909. A score in this range corresponds to a <0.5% error rate in base calling. These results suggested that this novel mutation may be observable in more CPP tumors. The Polyphen score indicates whether a substitution is damaging, and predicts the possible impact of an amino acid substitution on the structure and function of a human protein. Variants with Polyphen scores in the range of 0.0-0.15 are predicted to be benign, with the score of 0.15-1.0 potentially having a damaging effect, and 0.85-1.0 score established as damaging (23). The novel ATM variant revealed in the present study had a Polyphen score of 0.097, which suggested that it may be benign.

Numerous ATM mutants possess the ability to autophosphorylate on Ser-1981 (73). This activation by the autophosphorylation on Ser1981 leads to dissociation of the inactive ATM dimer (or higher-order multimer) into single protein molecules with kinase activity (51). Most missense mutations occur in the C-terminal part of the amino acid 1966. Mutations of the N-terminal part are therefore less likely to result in loss of kinase activity (74). The novel mutation found in this study was Leu1936Phe that was between the autophosphorylation sites viz, Ser1893 and Ser1981 (73). This result suggested that the kinase activity of ATM protein may not be affected by this mutation, since the kinase domain in ATM

was situated between the amino acids 2712 and 2962. Also FRAP/ATM/TRRAP (FAT) domain is not affected because it is at region 1960 to 2566 amino acids (51).

In conclusion, the present study identified a novel ATM mutation and 11 novel mutations in an a-CPP tumor, which had not yet been reported in any databases. Since these novel mutations have not been previously implicated in choroid plexus tumors, the findings from the present study may reveal a genetic signature that could be useful to distinguish choroid plexus tumors between CPP, a-CPP and CPC. In addition, the present study was the first reported case of a-CPP from Saudi Arabia. In this tumor, EGFR mutations were detected in the kinase and autophosphorylation domains of EGFR. The presence of mutations in this driver gene may indicate the transformation of a a-CPP grade II tumor to a CPC grade III tumor. Furthermore, the present study revealed mutations in KDM5C, PARP, SMARCA4 and ATM genes, which suggested that they may serve crucial role in chromatin remodeling, and may serve in understanding the progression of the benign tumor to malignant tumor. The results from this study may help the development of targeted therapies for this pediatric tumor, which had not been previously due to the lack of mutational information. This investigation may allow understanding this rare tumor at a molecular level.

## Acknowledgements

## Availability of data and materials

The datasets generated during the current study are available from the corresponding author on reasonable request.

## Authors' contributions

THN and AB collected the data. MS, ZA and AAH provided formal analysis of the results. Data curation was done by RAJ and HA. The study was investigated by GD and MA. The methodology of the current study was designed by WME, GD and MMT. The original draft of the manuscript was written by MMT and MS.

## Ethics approval and consent to participate

This study was approved by the Institutional Review Board for Bioethics Committee of King Abdullah Medical City, Makkah, Kingdom of Saudi Arabia (IRB no. 14-140), and performed in accordance with the principles of the Declaration of Helsinki. Informed consent was obtained from the guardian of the patient prior to the study.

## Patient consent for publication

Not applicable.

## Competing interests

All authors agreed with the contents of this manuscript and declare that they have no competing interests.

## References

1. Safaee M, Oh MC, Bloch O, Sun MZ, Kaur G, Auguste KI, Tihan T and Parsa AT: Choroid plexus papillomas: Advances in molecular biology and understanding of tumorigenesis. Neuro Oncol 15: 255-267, 2013.
2. Ellenbogen RG, Winston KR and Kupsky WJ: Tumors of the choroid plexus in children. Neurosurgery 25: 327-335, 1989.
3. Rickert CH and Paulus W: Tumors of the choroid plexus. Microsc Res Tech 52: 104-111, 2001.
4. Louis DN, Perry A, Reifenberger G, von Deimling A, Figarella-Branger D, Cavenee WK, Ohgaki H, Wiestler OD, Kleihues P and Ellison DW: The 2016 World Health Organization Classification of tumors of the central nervous system: A summary. Acta Neuropathol 131: 803-820, 2016.
5. Jaiswal S, Vij M, Mehrotra A, Kumar B, Nair A, Jaiswal AK, Behari S and Jain VK: Choroid plexus tumors: A clinico-pathological and neuro-radiological study of 23 cases. Asian J Neurosurg 8: 29-35, 2013.
6. Lechanoine F, Zemmoura I and Velut S: Treating cerebrospinal fluid rhinorrhea without dura repair: A case report of posterior fossa choroid plexus papilloma and review of the literature. World Neurosurg 108: 990.e1-990.e9, 2017.
7. Wolff JE, Sajedi M, Coppes MJ, Anderson RA and Egeler RM: Radiation therapy and survival in choroid plexus carcinoma. Lancet 353: 2126, 1999.
8. Park SH, Won J, Kim SI, Lee Y, Park CK, Kim SK and Choi SH: Molecular testing of brain tumor. J Pathol Transl Med 51: 205-223, 2017.
9. Custodio G, Taques GR, Figueiredo BC, Gugelmin ES, Oliveira Figueiredo MM, Watanabe F, Pontarolo R, Lalli E and Torres LF: Increased incidence of choroid plexus carcinoma due to the germline TP53 R337H mutation in southern Brazil. PLoS One 6: e18015, 2011.
10. Østrup O, Nysom K, Scheie D, Schmidt AY, Mathiasen R, Hjalgrim LL, Olsen TE, Skjøth-Rasmussen J, Henriksen BM, Nielsen FC, *et al*: Importance of comprehensive molecular profiling for clinical outcome in children with recurrent cancer. Front Pediatr 6: 114, 2018.
11. Merino DM, Shlien A, Villani A, Pienkowska M, Mack S, Ramaswamy V, Shih D, Tatevossian R, Novokmet A, Choufani S, *et al*: Molecular characterization of choroid plexus tumors reveals novel clinically relevant subgroups. Clin Cancer Res 21: 184-192, 2015.
12. Hasselblatt M, Böhm C, Tatenhorst L, Dinh V, Newrzella D, Keyvani K, Jeibmann A, Buerger H, Rickert CH and Paulus W: Identification of novel diagnostic markers for choroid plexus tumors: A microarray-based approach. Am J Surg Pathol 30: 66-74, 2006.
13. Sevenet N, Sheridan E, Amram D, Schneider P, Handgretinger R and Delattre O: Constitutional mutations of the hSNF5/INI1 gene predispose to a variety of cancers. Am J Hum Genet 65: 1342-1348, 1999.
14. Mueller W, Eum JH, Lass U, Paulus W, Sarkar C, Bruck W and von Deimling A: No evidence of hSNF5/INI1 point mutations in choroid plexus papilloma. Neuropathol Appl Neurobiol 30: 304-307, 2004.
15. Phelan ML, Sif S, Narlikar GJ and Kingston RE: Reconstitution of a core chromatin remodeling complex from SWI/SNF subunits. Mol Cell 3: 247-253, 1999.
16. Reisman D, Glaros S and Thompson EA: The SWI/SNF complex and cancer. Oncogene 28: 1653-1668, 2009.

17. Kreiger PA, Judkins AR, Russo PA, Biegel JA, Lestini BJ, Assanasen C and Pawel BR: Loss of INI1 expression defines a unique subset of pediatric undifferentiated soft tissue sarcomas. Mod Pathol 22: 142-150, 2009.
18. de Jong MM, Nolte IM, Meerman GJ, van der Graaf WT, Oosterwijk JC, Kleibeuker JH, Schaapveld M and de Vries EG: Genes other than BRCA1 and BRCA2 involved in breast cancer susceptibility. J Med Genet 39: 225-242, 2002.
19. Miyagi K, Mukawa J, Kinjo N, Horikawa K, Mekaru S, Nakasone S, Koga H, Higa Y and Naito M: Astrocytoma linked to familial ataxia-telangiectasia. Acta Neurochir (Wien) 135: 87-92, 1995.
20. Piane M, Molinaro A, Soresina A, Costa S, Maffeis M, Germani A, Pinelli L, Meschini R, Plebani A, Chessa L and Micheli R: Novel compound heterozygous mutations in a child with Ataxia-Telangiectasia showing unrelated cerebellar disorders. J Neurol Sci 371: 48-53, 2016.
21. Cryan JB, Haidar S, Ramkissoon LA, Bi WL, Knoff DS, Schultz N, Abedalthagafi M, Brown L, Wen PY, Reardon DA, et al: Clinical multiplexed exome sequencing distinguishes adult oligodendroglial neoplasms from astrocytic and mixed lineage gliomas. Oncotarget 5: 8083-8092, 2014.
22. Pécuchet N, Zonta E, Didelot A, Combe P, Thibault C, Gibault L, Lours C, Rozenholc Y, Taly V, Laurent-Puig P, et al: Base-position error rate analysis of next-generation sequencing applied to circulating tumor DNA in non-small cell lung cancer: A prospective study. PLoS Med 13: e1002199, 2016.
23. Adzhubei IA, Schmidt S, Peshkin L, Ramensky VE, Gerasimova A, Bork P, Kondrashov AS and Sunyaev SR: A method and server for predicting damaging missense mutations. Nat Methods 7: 248-249, 2010.
24. Han CM, Hwang Y, Kim CK and Oh JH: Genetic profile analysis of a patient with metachronous gastric cancer with a family history of gastrointestinal cancers. Korean J Helicobacter Upper Gastrointest Res 17: 218-223, 2017.
25. Chakrabarty S, Varghese VK, Sahu P, Jayaram P, Shivakumar BM, Pai CG and Satyamoorthy K: Targeted sequencing-based analyses of candidate gene variants in ulcerative colitis-associated colorectal neoplasia. Br J Cancer 117: 136-143, 2017.
26. Wrede B, Hasselblatt M, Peters O, Thall PF, Kutluk T, Moghrabi A, Mahajan A, Rutkowski S, Diez B, Wang X, et al: Atypical choroid plexus papilloma: Clinical experience in the CPT-SIOP-2000 study. J Neurooncol 95: 383-392, 2009.
27. Adesina AM: Intraoperative consultation in the diagnosis of pediatric brain tumors. Arch Pathol Lab Med 129: 1653-1660, 2005.
28. Uff CE, Galloway M and Bradford R: Metastatic atypical choroid plexus papilloma: A case report. J Neurooncol 82: 69-74, 2007.
29. Singh A, Vermani S, Sharma S and Chand K: Papillary meningioma: A rare but distinct variant of malignant meningioma. Diagn Pathol 2: 3, 2007.
30. Jamjoom AA, Sharab MA, Jamjoom AB and Satti MB: Rapid evolution of a choroid plexus papilloma in an infant. Br J Neurosurg 23: 324-325, 2009.
31. Japp AS, Gessi M, Messing-Jünger M, Denkhaus D, Zur Mühlen A, Wolff JE, Hartung S, Kordes U, Klein-Hitpass L and Pietsch T: High-resolution genomic analysis does not qualify atypical plexus papilloma as a separate entity among choroid plexus tumors. J Neuropathol Exp Neurol 74: 110-120, 2015.
32. Matsushima T, Inoue T, Takeshita I, Fukui M, Iwaki T and Kitamoto T: Choroid plexus papillomas: An immunohistochemical study with particular reference to the coexpression of prealbumin. Neurosurgery 23: 384-389, 1988.
33. Sameshima T, Tanikawa R, Sugimura T, Izumi N, Seki T, Maeda T, Tsuboi T, Hashimoto M, Kimura T and Nabeshima K: Choroid plexus papilloma originating in the sella turcica-case report. Neurol Med Chir (Tokyo) 50: 144-146, 2010.
34. Figarella-Branger D, Lepidi H, Poncet C, Gambarelli D, Bianco N, Rougon G and Pellissier JF: Differential expression of cell adhesion molecules (CAM). neural CAM and epithelial cadherin in ependymomas and choroid plexus tumors. Acta Neuropathol 89: 248-257, 1995.
35. Kim SA, Inamura K, Yamauchi M, Nishihara R, Mima K, Sukawa Y, Li T, Yasunari M, Morikawa T, Fitzgerald KC, et al: Loss of CDH1 (E-cadherin) expression is associated with infiltrative tumour growth and lymph node metastasis. Br J Cancer 114: 199-206, 2016.
36. Gumbiner BM: Regulation of cadherin-mediated adhesion in morphogenesis. Nat Rev Mol Cell Biol 6: 622-634, 2005.
37. Losi-Guembarovski R, Kuasne H, Guembarovski AL, Rainho CA and Cólus IM: DNA methylation patterns of the CDH1. RARB. and SFN genes in choroid plexus tumors. Cancer Genet Cytogenet 179: 140-145, 2007.
38. Hirohashi S and Kanai Y: Cell adhesion system and human cancer morphogenesis. Cancer Sci 94: 575-581, 2003.
39. Lv SQ, Song YC, Xu JP, Shu HF, Zhou Z, An N, Huang QL and Yang H: A novel TP53 somatic mutation involved in the pathogenesis of pediatric choroid plexus carcinoma. Med Sci Monit 18: CS37-CS41, 2012.
40. Tabori U, Shlien A, Baskin B, Levitt S, Ray P, Alon N, Hawkins C, Bouffet E, Pienkowska M, Lafay-Cousin L, et al: TP53 alterations determine clinical subgroups and survival of patients with choroid plexus tumors. J Clin Oncol 28: 1995-2001, 2010.
41. Vital A, Bringuier PP, Huang H, San Galli F, Rivel J, Ansoborlo S, Cazauran JM, Taillandier L, Kleihues P and Ohgaki H: Astrocytomas and choroid plexus tumours in two families with identical p53 germline mutations. J Neuropathol Exp Neurol 57: 1061-1069, 1998.
42. Bettegowda C, Agrawal N, Jiao Y, Wang Y, Wood LD, Rodriguez FJ, Hruban RH, Gallia GL, Binder ZA, Riggins CJ, et al: Exomic sequencing of four rare central nervous system tumor types. Oncotarget 4: 572-583, 2013.
43. Synhaeve NE, van den Bent MJ, French PJ, Dinjens WNM, Atmodimedjo PN, Kros JM, Verdijk R, Dirven CMF and Dubbink HJ: Clinical evaluation of a dedicated next generation sequencing panel for routine glioma diagnostics. Acta Neuropathol Commun 6: 126, 2018.
44. Brastianos PK, Taylor-Weiner A, Manley PE, Jones RT, Dias-Santagata D, Thorner AR, Lawrence MS, Rodriguez FJ, Bernardo LA, Schubert L, et al: Exome sequencing identifies BRAF mutations in papillary craniopharyngiomas. Nat Genet 46: 161-165, 2014.
45. Merchant M, Evangelista M, Luoh SM, Frantz GD, Chalasani S, Carano RA, van Hoy M, Ramirez J, Ogasawara AK, McFarland LM, et al: Loss of the serine/threonine kinase fused results in postnatal growth defects and lethality due to progressive hydrocephalus. Mol Cell Biol 25: 7054-7068, 2005.
46. Shajani-Yi Z, de Abreu FB, Peterson JD and Tsongalis GJ: Frequency of somatic TP53 mutations in combination with known pathogenic mutations in colon adenocarcinoma, non-small cell lung carcinoma and gliomas as identified by next-generation sequencing. Neoplasia 20: 256-262, 2018.
47. Parsons DW, Jones S, Zhang X, Lin JC, Leary RJ, Angenendt P, Mankoo P, Carter H, Siu IM, Gallia GL, et al: An integrated genomic analysis of human glioblastoma multiforme. Science 321: 1807-1812, 2008.
48. The Cancer Genome Atlas Research Network: Comprehensive genomic characterization defines human glioblastoma genes and core pathways. Nature 455: 1061-1068, 2008.
49. Rath PB, Lal O, Ajala Y, Li Y, Xia S, Kim J and Laterra J: In vivo c-Met pathway inhibition depletes human glioma xenografts of tumor-propagating stem-like cells. Transl Oncol 6: 104-111, 2013.
50. Hasselblatt M, Gesk S, Oyen F, Rossi S, Viscardi E, Giangaspero F, Giannini C, Judkins AR, Frühwald MC, Obser T, et al: Nonsense mutation and inactivation of SMARCA4 (BRG1) in an atypical teratoid/rhabdoid tumor showing retained SMARCB1 (INI1) expression. Am J Surg Pathol 35: 933-935, 2011.
51. Bakkenist CJ and Kastan MB: DNA damage activates ATM through intermolecular autophosphorylation and dimer dissociation. Nature 421: 499-506, 2003.
52. Kozlov SV, Graham ME, Jakob B, Tobias F, Kijas AW, Tanuji M, Chen P, Robinson PJ, Taucher-Scholz G, Suzuki K, et al: Autophosphorylation and ATM activation: Additional sites add to the complexity. J Biol Chem 286: 9107-9119, 2011.
53. Hirsch P, Zhang Y, Tang R, Joulin J, Boutroux H, Pronier E, Moatti H, Flandrin P, Marzac C, Bories D, et al: Genetic hierarchy and temporal variegation in the clonal history of acute myeloid leukaemia. Nat Commun 7: 12475, 2016.
54. Beschorner R, Waidelich J, Trautmann K, Psaras T and Schittenhelm J: Notch receptors in human choroid plexus tumors. Histol Histopathol 28: 1055-1063, 2013.
55. Ricks TK, Chiu HJ, Ison G, Kim G, McKee AE, Kluetz P and Pazdur R: Successes and challenges of PARP inhibitors in cancer therapy. Front Oncol 5: 222, 2015.
56. Ray Chaudhuri A and Nussenzweig A: The multifaceted roles of PARP1 in DNA repair and chromatin remodelling. Nat Rev Mol Cell Biol 18: 610-621, 2017.
57. Gros-Louis F, Dupré N, Dion P, Fox MA, Laurent S, Verreault S, Sanes JR, Bouchard JP and Rouleau GA: Mutations in SYNE1 lead to a newly discovered form of autosomal recessive cerebellar ataxia. Nat Genet 39: 80-85, 2007.
58. Masica DL and Karchin R: Correlation of somatic mutation and expression identifies genes important in human glioblastoma progression and survival. Cancer Res 71: 4550-4561, 2011.

59. Weng AP, Ferrando AA, Lee W, Morris JP IV, Silverman LB, Sanchez-Irizarry C, Blacklow SC, Look AT and Aster JC: Activating mutations of NOTCH1 in human T cell acute lymphoblastic leukemia. Science 306: 269-271, 2004.
60. Espinoza I and Miele L: Notch inhibitors for cancer treatment. Pharmacol Ther 139: 95-110, 2013.
61. Lee SY, Kumano K, Masuda S, Hangaishi A, Takita J, Nakazaki K, Kurokawa M, Hayashi Y, Ogawa S and Chiba S: Mutations of the Notch1 gene in T-cell acute lymphoblastic leukemia: Analysis in adults and children. Leukemia 19: 1841-1843, 2005.
62. Sheardown S, Norris D, Fisher A and Brockdorff N: The mouse Smcx gene exhibits developmental and tissue specific variation in degree of escape from X inactivation. Hum Mol Genet 5: 1355-1360, 1996.
63. Wlodarski MW, Collin M and Horwitzd MS: GATA2 deficiency and related myeloid neoplasms. Semin Hematol 54: 81-86, 2017.
64. Rodriguez-Bravo V, Carceles-Cordon M, Hoshida Y, Cordon-Cardo C, Galsky MD and Domingo-Domenech J: The role of GATA2 in lethal prostate cancer aggressiveness. Nat Rev Urol 14: 38-48, 2017.
65. Kastan MB and Lim DS: The many substrates and functions of ATM. Nat Rev Mol Cell Biol 1: 179-186, 2000.
66. Blake SM, Stricker SH, Halavach H, Poetsch AR, Cresswell G, Kelly G, Kanu N, Marino S, Luscombe NM, Pollard SM and Behrens A: Inactivation of the ATMIN/ATM pathway protects against glioblastoma formation. Elife 5: e08711, 2016.
67. Eich M, Roos WP, Nikolova T and Kaina B: Contribution of ATM and ATR to the resistance of glioblastoma and malignant melanoma cells to the methylating anticancer drug temozolomide. Mol Cancer Ther 12: 2529-2540, 2013.
68. Maréchal A and Zou L: DNA damage sensing by the ATM and ATR kinases. Cold Spring Harb Perspect Biol 5: a012716, 2013.
69. Biddlestone-Thorpe L, Sajjad M, Rosenberg E, Beckta JM, Valerie NC, Tokarz M, Adams BR, Wagner AF, Khalil A, Gilfor D, *et al*: ATM kinase inhibition preferentially sensitizes p53 mutant glioma to ionizing radiation. Clin Cancer Res 19: 3189-3200, 2013.
70. Zou Y, Wang Q, Li B, Xie B and Wang W: Temozolomide induces autophagy via ATM-AMPK-ULK1 pathways in glioma. Mol Med Rep 10: 411-416, 2014.
71. Janin N, Andrieu N, Ossian K, Laugé A, Croquette MF, Griscelli C, Debré M, Bressac-de-Paillerets B, Aurias A and Stoppa-Lyonnet D: Breast cancer risk in ataxia telangiectasia (AT) heterozygotes: Haplotype study in French AT families. Br J Cancer 80: 1042-1045, 1999.
72. Carson AR, Smith EN, Matsui H, Brækkan SK, Jepsen K, Hansen JB and Frazer KA: Effective filtering strategies to improve data quality from population-based whole exome sequencing studies. BMC Bioinformatics 15: 125, 2014.
73. Khalil HS, Tummala H and Zhelev N: ATM in focus: A damage sensor and cancer target. Biodiscov 5: 1, 2012.
74. Lavina MF, Scotta S, Guevena N, Kozlova S, Penga C and Chena P: Functional consequences of sequence alterations in the ATM gene. DNA Repair (Amst) 3: 1197-1205, 2004.